

The link between molecular cloud structure and turbulence

N. Schneider¹, S. Bontemps², R. Simon³, V. Ossenkopf³, C. Federrath^{4,5}, R. Klessen⁴, F. Motte¹, and C. Brunt⁶

¹ IRFU/SAP CEA/DSM, Laboratoire AIM CNRS - Université Paris Diderot, 91191 Gif-sur-Yvette, France

² OASU/LAB-UMR5804, CNRS, Université Bordeaux 1, 33270 Floirac, France

³ I. Physikalisches Institut, Universität zu Köln, Zùlpicher Straße 77, 50937 Köln, Germany

⁴ Zentrum für Astronomie der Universität Heidelberg, Inst. für Theor. Astrophysik, Albert-Ueberle Str. 2, 69120 Heidelberg, Germany

⁵ Max-Planck-Institute for Astronomy, Königstuhl 17, 69117 Heidelberg, Germany

⁶ School of Physics, University of Exeter, Exeter, EX4QL, UK

May 2, 2019

ABSTRACT

Aims. We aim to better understand how the spatial structure of molecular clouds is governed by turbulence. For that, we study the large-scale spatial distribution of low density molecular gas and search for characteristic length scales.

Methods. We employ a 35 square degrees ¹³CO 1→0 molecular line survey of Cygnus X and visual extinction (A_V) maps of 17 Galactic clouds to analyse the spatial structure using the Δ -variance method.

Results. The Δ -variance spectra obtained from the A_V maps show differences between low-mass star forming (SF) clouds and massive giant molecular clouds (GMC) in terms of shape of the spectrum and values of the slope β . Low-mass SF clouds have a double-peak structure with characteristic size scales around 1 pc and 4 pc. These scales may represent SF molecular clumps (1 pc) and/or the width (1 pc) and length (4 pc) of filaments. GMCs show no characteristic scale in the A_V -maps which can partly be ascribed to a distance effect due to a larger line-of-sight (LOS) confusion. The Δ -variance for Cygnus, determined from the ¹³CO survey, shows characteristic scales at 4 pc and 40 pc, either reflecting the filament structure and large-scale turbulence forcing or – for the 4 pc scale – the threshold scale when the ¹³CO 1→0 line becomes optically thick. Though there are different reasons for characteristic scales (geometry, decaying turbulence, LOS-effects and energy injection due to expanding supernova shells, outflows, etc.), and the relative contribution of these effects strongly varies from cloud to cloud, it is remarkable that the resulting turbulent structure of molecular clouds shows similar characteristics.

Key words. interstellar medium: clouds – individual objects: Cygnus X – molecules – kinematics and dynamics – Radio lines: ISM

1. Introduction

Turbulence

Over the last years, much progress has been made to theoretically explain the observational claim that *turbulence* governs the different phases of the Interstellar Medium (ISM). Molecular line surveys of molecular clouds as a whole led to the detection of the linewidth-size $\sigma \propto L^\epsilon$ and mass-size $M \propto L^\gamma$ relations (Larson 1981) with $\epsilon \sim 0.2...0.5$ and $\gamma \sim 2$ (e.g. Goldsmith 1987, Heyer & Brunt 2004), and a mass distribution for molecular clumps of the form of $dN/dM \sim M^{-\alpha}$ with $\alpha \sim 1.5-1.9$ (e.g. Kramer et al. 1998). The spatial structure of the emission has been characterized in terms of power spectra (Scalo 1987, Stutzki et al. 1998).

The scaling relations and power laws can be explained in the context of turbulence, where energy is injected at very large scales and cascades down to the smallest scales, creating eddies and stirring up the cloud. The driving sources for turbulence on the largest scales can be diverse, ranging from supernova explosions (MacLow & Klessen 2004, Dib et al. 2009) to turbulence that is generated during the formation process of molecular clouds which are proposed to form at the convergence of large-scale flows in the atomic phase (Vazquez-Semadeni 2007, Heitsch et al. 2008). Recently, Brunt et al. (2009) showed that the size-velocity dispersion of giant molecular clouds can only be reproduced in case of turbulence driven on large scales.

In its simplest form, the Kolmogorov-turbulence (Kolmogorov 1941) describes an incompressible, non-magnetic fluid in which the statistical properties of the flow are independent of the scale within the inertial range. This leads to an index of $\epsilon=0.33$ and to a self-similar, i.e. *fractal*, spatial structure. Other turbulence fluid models (Vazquez-Semadeni et al. 1997, Ballesteros-Paredes & MacLow 2002, Federrath et al. 2009), describing a supersonic, isothermal turbulent flow obtain $\epsilon=0.5$ and $\gamma=2$. Hennebelle & Audit (2007) and Hennebelle, Audit, Miville-Deschenes (2007) take a different approach and describe turbulence by the individual motion of cloudlets. Their hydrodynamic, non-magnetic, non-self-gravitating simulations of a turbulent 2D-phase of atomic HI gas led to a mass-size relation of $M \sim L^{1.7}$ and a clump mass spectral index $\alpha \approx 1.7$, a value similar to that found for CO clumps.

These few examples show already the effort that is made to take into account the complexity of the ISM and to compare observations with theory. However, each model represents a particular physical situation with different accentuations of the various physical effects that play a role (driving source of turbulence, magnetic fields, self-gravity, thermal balance, etc.). In particular the importance of *self-gravity* was pointed out by, e.g. Vazquez-Semadeni et al. (2008), emphasizing that a part of the observed velocity dispersion in molecular clouds is due to clump-scale inward motions as a consequence of gravitational collapse and not turbulence. Bonnell et al. 2006) question the scenario where continuously driven turbulence generates the density inhomogeneities in star-forming clouds. Instead, they

Send offprint requests to: N. Schneider

Correspondence to: nschneid@cea.fr

find that it is the primordial clumpiness of the interstellar gas that produces turbulence as it passes through the spiral shock and initiates the star formation process. Clark & Bonnell (2006) suggest that turbulence only provides shocks that dissipate the supporting kinetic energy and generate structure which acts as seeds for the subsequent fragmentation. This would naturally explain the formation of multiple systems. Recent hydrodynamic models (Bate 2009) stress the importance of *radiative feedback processes* from stars that can drastically reduce the total number of stars formed. These ‘deviations’ from the idealized scenario of a purely turbulent medium may cause changes of the scaling laws. This could explain, for example, why many molecular line studies failed to detect a linewidth-size relation in molecular *clumps* (e.g. Loren 1989, Simon et al. 2001, Schneider & Brooks 2004).

Molecular cloud structure

The observed spatial structure of molecular clouds depends on the tracer used to image the clouds. Low-J rotational transitions of ^{12}CO or visual extinction maps are sensitive to low densities and show a very complex structure that – with a change to higher angular resolution – breaks up into substructures, which appear similar on almost all scales (e.g., Falgarone et al. 1991, Stutzki 2001). The concept of ‘self-similarity’ as a geometrical property was introduced (Elmegreen & Falgarone 1996) and this gas component is well described as a fractal-Brownian-motion (fBM) structure (Stutzki et al. 1998). In contrast, gas at much higher column density, best traced by dust (sub)mm-continuum emission or molecular line high density tracers like CS, shows no fractal structure (Falgarone et al. 2004). In addition, self-similarity may break down on the smallest scales (<0.1 pc), relevant for star formation (e.g. Goodman et al. 1998, Dib et al. 2008, Federrath et al. 2009).

However, it is difficult to transform model results into ‘observables’ such as the 3D- or projected (on the plane of the sky) emission and velocity structure of an observed molecular line. Ballesteros-Paredes & Mac Low (2002) argued that the apparent mass-size relation is due to the observations and/or the analysis process: any cutoff in column density, due to the limited dynamic range and/or the minimum intensity level defined by clump finding algorithms automatically implies $M \propto L^2$. Even more problematic is the velocity superposition of many clumps in the line-of-sight when a low-density tracer like ^{12}CO is used. High-density tracers like CS or N_2H^+ provide a better clump separation but imply a bias in analysing the full cloud structure (only the densest structures are identified). A survey using the ^{13}CO line may be the best compromise.

Describing molecular cloud structure

Statistical tools have been developed to analyse the observed spatial and kinematic cloud structure, which turns out to be extremely complex. Amongst the most commonly used tools to describe structure are probability distribution functions of line intensities (Padoan et al. 1997), the Δ -variance analysis of intensities and velocities (Stutzki et al. 1998, Ossenkopf 2002), and the principal component analysis (Heyer & Schloerb 1997). In this study, we use the Δ -variance method, applied to a large ^{13}CO $1 \rightarrow 0$ survey obtained with the FCRAO¹ 14m telescope of the Cygnus X region and on a data set of 17 near-IR extinction maps of molecular clouds derived from 2MASS. This analysis will help to further develop and refine models and cloud structure characterization techniques. We are

particularly interested to see whether there is a dependence of cloud characteristics (size scales, value of the power-law slope β , form of the Δ -variance spectrum) and cloud type (low- and high-mass star-forming molecular clouds, diffuse gas).

Cygnus X

The Cygnus X region is the richest and most massive complex of high-mass star formation at a distance lower than 3 kpc. Schneider et al. (2006, 2007) showed that the Cygnus X region constitutes a large scale network of GMCs at a common distance of ~ 1.7 kpc. Signposts of recent and ongoing (high-mass) star formation (H II regions, outflow activity, IR-sources such as S106 IR, DR21, W75N, and GL2591) are ubiquitous. See Schneider et al. (2006) or Reipurth & Schneider (2008) for a review on Cygnus X. The region also contains several OB clusters (Cyg OB1–4, 6, and 8) including the richest known OB cluster of the Galaxy, Cyg OB2 (Knödlseider 2000, Uyaniker et al. 2001). Their energy injection from stellar winds and radiation could be a driving source for turbulence.

2. Observations

2.1. FCRAO ^{13}CO $1 \rightarrow 0$ survey

The data presented here were obtained using the FCRAO partly in remote operation from late 2003 to early 2006. The summer period was excluded for observations due to weather constraints. The molecular lines of ^{13}CO $1 \rightarrow 0$ at 110.201 GHz and C^{18}O $1 \rightarrow 0$ at 109.782 GHz were observed simultaneously. The beamwidth of the FCRAO at 110 GHz is $46''$.

A total of 35 square degrees in Cygnus X was covered in the ^{13}CO and C^{18}O $1 \rightarrow 0$ lines at $46''$ angular resolution (Simon et al., in prep.). This survey is significantly larger and at higher angular resolution than the ^{13}CO $2 \rightarrow 1$ map presented by Schneider et al. (2007). It has a spectral dynamic range (maximum observed linewidth over velocity resolution) of ~ 70 and a spatial dynamic range (map size over angular resolution) of ~ 230 . This is much larger than what is usually obtained for molecular cloud maps (Kramer et al. 1998). The highest column density regions traced in the FCRAO ^{13}CO $1 \rightarrow 0$ survey were then observed in the CS $2 \rightarrow 1$ and N_2H^+ $1 \rightarrow 0$ lines (~ 15 square degrees) using the FCRAO.

Pointing and calibration were checked regularly at the start of the Cygnus observing time interval and after transit of Cygnus (no observations were performed at elevations higher than 75°). Pointing sources were SiO masers of evolved stars, i.e., χ -Cyg, R-Leo and T-Cep, depending on observing time. The calibration was checked regularly on the position of peak emission in DR21 and found to be consistent within 10%.

We used the single sideband focal plane array receiver SEQUOIA (Second Quabbin Optical Imaging Array; Erickson et al. 1999) designed for the 85–115.6 GHz range, yielding a mean receiver noise temperature of 60 K. SEQUOIA is a 4×4 dual-polarization array with a separation between elements of $88''$ on the sky. The receiver was used in combination with a dual channel correlator (DCC), configured to a bandwidth of 25 MHz, using 1024 channels, corresponding to a velocity sampling of 0.066 km s^{-1} .

We used the on-the-fly mapping mode (OTF) in which each map consisted of a block of $20' \times 10'$ (30 minutes integration time including overheads). The data quality is enhanced because pixel-to-pixel variations are averaged in the final regridded data set. Since at the map edges the coverage is less dense, and thus

¹ Five College Radio Astronomy Observatory

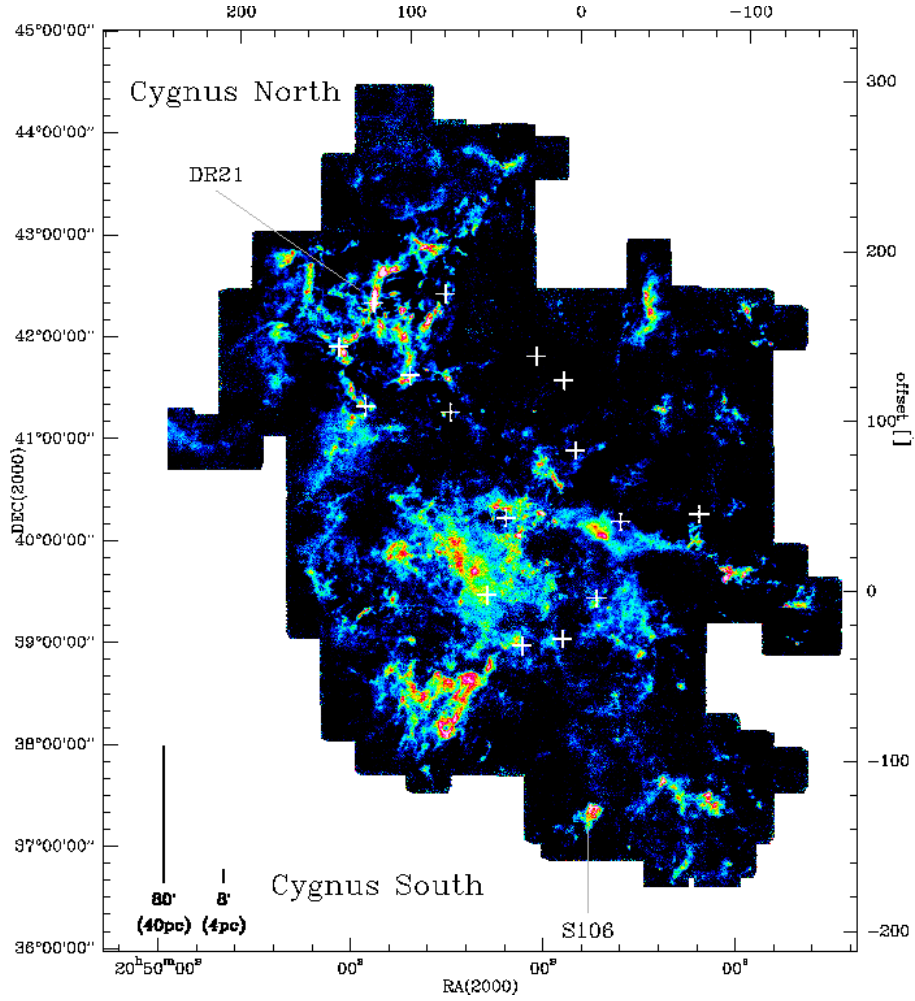


Fig. 1. Line integrated map of Cygnus X in ^{13}CO 1 \rightarrow 0 emission with the intensity (-1 to 16 K km s^{-1}) coded in color. Crosses indicate the location of thermal HII regions, the well-known star-forming regions DR21 and S106 are labelled.

leads to an increase in noise, adjacent maps were overlapping to cover the region at uniform density.

In total, $\sim 800,000$ spectra were produced on $22''.5$ sampled grid covering an area of 35 deg^2 . The data have a mean $1 \sigma_{\text{rms}}$ rms noise level of $\sim 0.2 \text{ K}$ per 0.06 km s^{-1} channel on a T_A^* antenna temperature scale, i.e., not corrected for the main beam efficiency of ~ 0.48 . More details on the observing procedure, regridding and the rms-map of ^{13}CO are found in Appendix A and in Simon et al., in prep..

2.2. Near-Infrared extinction maps

The basic idea of deriving extinction maps from near-infrared (near-IR) data is that the average reddening of background stars, as observed in the near-IR bands (usually J, H and K), is used to estimate the total column density of dust along the line-of-sight and thus the total A_V in that direction (e.g. Lada et al. 1994).

We developed a new technique (AvMAP) to produce in an efficient way extinction maps from the 2MASS² catalog following the schemes described in Lombardi et al. (2001) and

Cambresy et al. (2002), but with the improvements that (i) it is a fast algorithm which can easily handle large fields with millions of sources, (ii) include a calibration of the extinction which does not require an off-field, and (iii) it is a method to estimate the density of foreground stars which follows the spatial distribution of stars in the Galaxy by using the predictions of the stellar population model of Besançon (Robin et al. 2003; see <http://model.obs-besancon.fr/>) to filter out foreground stars. Thus, A_V -maps can be produced up to a distance of 3 kpc at an angular resolution of typically $2''$. A detailed description of the method is given in the appendix.

3. The Δ -Variance as a method of structure analysis

3.1. Definition of Δ -variance

The Δ -variance is a method to analyze the structure and correlation in multi-dimensional scalar functions. It was first introduced by Stutzki et al. (1998), who expanded the 1-D Allan variance concept (Allan 1966) to two and more dimensions in order to characterize the observed 2-D structure in molecular cloud images.

² The Two Micron All Sky Survey (2MASS) is a joint project of the University of Massachusetts and the Infrared Processing and Analysis Center/California Institute of Technology, funded by the National Aeronautics and Space Administration and the National Science Foundation.

The Δ -variance³ measures the amount of structure on a given scale L in a map s (2-dimensional scalar function) by filtering this map with a spherically symmetric wavelet \bigcirc_L :

$$\sigma_{\Delta}^2(L) = \langle (s \otimes \bigcirc_L)^2 \rangle_{x,y}$$

The Δ -variance thus probes the variation of the intensity s over a length L (called *lag*), i.e., the amount of structural variation on that scale. The filter function can vary between a smooth or a step-shaped filter function ('Mexican hat' or 'French hat'). Ossenkopf et al. (2008a) analysed systematically (using simulations) the influence of the shape of the filter function and arrived to the conclusion that the Mexican hat filter, with an annulus-to-core-diameter ratio of about 1.5, provided the best results for a clear detection of pronounced scales.

The observed structure can be well mimicked by a *fractional Brownian motion (fBm)* structure (which has a power-law spectrum) in the context of fractal images. For any 2-D image with a power spectrum $P(k) \propto |k|^{-\beta}$, in which k is the spatial frequency, the 2-D Δ -variance varies as $\sigma_{\Delta}^2 \propto L^{\beta-2}$ for $0 < \beta < 6$ (see Stutzki et al. (1998) for more details). The range of L is given by the upper and lower spatial frequency cutoffs $k_u \approx (\Delta x)^{-1}$ and $k_l \approx (n\Delta x)^{-1}$ (Δx is the sampling grid of a map with n^2 pixels): $(2\pi k_u)^{-1} < L < (2\pi k_l)^{-1}$.

Noise contributions in the map can be separated from the intrinsic structure of the cloud because purely white noise has $\beta=0$ (flicker noise would lead to $\beta=1$). Weighting the image with the inverse noise function ($1/\sigma_{rms}$) enables to distinguish the variable noise from real small scale structure (see Bensch et al. 2001 for more details). At the smallest scales, the Δ -variance spectrum is dominated by the structure blurring from the finite telescope beam and radiometric noise.

Limitations of the Δ -variance – as it is the case for any structure analysis method – are obviously the resolution and the finite extent of the observed image, i.e., the shortest lag probed will be close to the angular resolution and the largest lag will be limited by the size of the image or the most extended emission.

4. Results

4.1. FCRAO ^{13}CO 1 \rightarrow 0 data

Figure 1 shows the line integrated map of Cygnus X in ^{13}CO 1 \rightarrow 0 emission, tracing gas densities around $3 \times 10^3 \text{ cm}^{-3}$. The main features seen in Cygnus X are high-contrast filaments, mainly in the northern part of the map (DR21), and more diffuse emission with some higher density clouds in the south. Schneider et al. (2006) named these two regions 'Cygnus North' and 'Cygnus South'. The molecular line emission from those clouds *related to the Cygnus X cloud complex* covers a velocity range between ~ -15 to $+20 \text{ km s}^{-1}$ (Schneider et al. 2006). However, some emission at velocities larger than $\sim 4 \text{ km s}^{-1}$ (Piepenbrink & Wendker 1988, Schneider et al. 2007) is due to the 'Great Cygnus Rift', a low-density gas feature at a distance of around 600 pc. It is responsible for a visual extinction of a few A_V (Dickel 1969, Schneider et al. 2007). In the figure, several arc or shell-like structures are visible, in particular in the northern part of the map where a cavity devoid of molecular gas (center at offsets 0', 120') is surrounded by clouds that may have formed as swept-up material from the HII regions and the influence of the OB2 cluster.

³ All Δ -variance calculations were performed using the IDL-based routine **deltavar** provided by V. Ossenkopf and available at www.astro.uni-koeln.de/ossk/ftpspace/delta

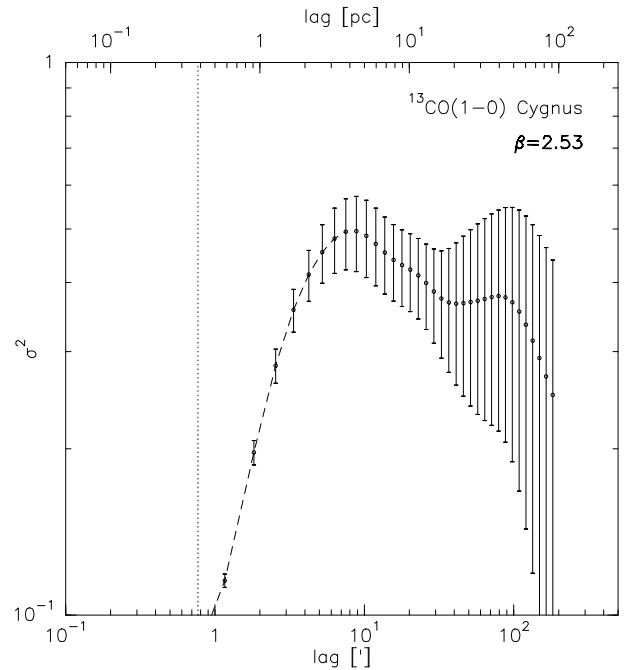


Fig. 2. The Δ -variance spectrum of the line integrated map of the *entire complex* in the ^{13}CO emission. The slope β is determined from a linear fit for data between lags 1' and 8' (indicated by a long-dashed line). The short-dashed line gives the beamsize (45'').

In order to show the variation in the amount of structure as a function of length (lag) in the clouds, we apply the Δ -variance method to the line integrated ^{13}CO 1 \rightarrow 0 map. This is the first time that a map of ~ 35 square degrees is analysed with the Δ -variance. Typical map sizes in previous studies (Bensch et al. 2001, Sun et al. 2006) were in the range of 1 to 10 square degrees. We profited from the $(1/\text{rms})$ weighting feature implemented in the Δ -variance algorithm developed by Ossenkopf et al. (2008a), so that areas with higher noise (in our case the map edges) contribute less to the Δ -variance than areas with low, uniform noise. This improves the accuracy of the results with respect to distinguishing real signal from noise.

Figure 2 shows the Δ -variance spectrum for the ^{13}CO 1 \rightarrow 0 map. The error of each $\sigma_{\Delta}^2(L)$ is determined from the Poisson statistics. The plot shows that with increasing lag L , the Δ -variance first increases and reaches its peak value at L_{peak} , i.e. 8' corresponding to 4 pc for a distance of 1.7 kpc. With increasing lag, a second peak is observed at 80' (40 pc) before the Δ -variance decreases approximately with L^{-2} . This spectrum⁴ does not represent a self-similar structure on all size scales (that would produce a pure power law) which originates from supersonic, driven turbulence (Mac Low & Ossenkopf 2000). *Characteristic scales* in a Δ -variance spectrum are due to (i) different geometrical scales (length and width of filaments for example), (ii) decaying turbulence (Mac Low & Ossenkopf 2000), (iii) energy injection from external or internal sources (supernovae, outflows, radiation pressure, etc.), or by (iv) superposition of different clouds along the line-of-sight (distance effect).

It is thus not straightforward to interpret the Δ -variance spectrum of Cygnus since several of these effects may play a role.

⁴ None of the scales corresponds to a structure introduced by the observational procedure because individual OTF-maps have a size of $10' \times 20'$.

First, it is known that at least two groups of molecular clouds at distances of 600 pc ('Great Rift') and 1.7 kpc (see above) are found in direction to Cygnus X. However, as shown and discussed in Schneider et al. (2007), the column density of the Rift gas is very low ($A_V < 3^m$) and not well traced by ^{13}CO emission. In this case, the whole Δ -variance spectrum would be due to emission features arising from the clouds in 1.7 kpc distance.

Characteristic scales due to energy injection are plausible since this region is strongly affected by radiation from the Cygnus OB2/OB9 clusters and a large number of outflow sources. However, one of the most important energy source are probably supernovae (MacLow & Klessen 2004) and the rate of SN-explosions in this area is very low (see overview in Reipurth & Schneider 2008). For example, no signatures of SN-shells were yet found in Cygnus X. One possible explanation for the spectrum is that with ^{13}CO , we trace well the cloud structure in terms of large and small filaments and clouds. The first peak around 4 pc corresponds well to the typical size scale found for nearby clouds (see section 4.2.2), characterizing a typical small filament size, while the second peak around 40 pc arises from the large filamentary structures clearly visible in Fig. 1. However, an alternative explanation is that the 4 pc scale is due to a radiative transfer effect in a turbulent medium (Padoan et al. 2000). As $^{13}\text{CO } 1 \rightarrow 0$ turns optically thick at column densities above about $N(\text{H}_2) = 10^{22} \text{ cm}^{-2}$ (Ossenkopf 2002), this tracer is not capable to resolve any denser structure and all peaks are blurred out. The ^{13}CO observations thus probably only provide a good reflection of the structure measured up to about $A_V = 5^m$. The peak in the ^{13}CO Δ -variance basically shows the typical size of the regions where the tracer turns optically thick, i.e. the ^{13}CO "photosphere" of the dense regions. The exact location of the peaks on the Δ -variance spectrum gives some measure for the turbulence in the molecular cloud. They indicate a transition from more coherent structures, where the ^{13}CO emission falls into a narrow velocity interval, to a wide-spread turbulent distribution leading to a dilution of the optical depth in very broad lines. The details of this transition will be studied in a subsequent paper based on the simultaneous Δ -variance analysis of the velocity structure.

The *power spectral index* β is typically determined for lags between the beamsize (indicated by a dashed line in Fig. 2) and the first significant structure component ($8'$). The value $\beta = 2.53$ is at the lower end of typical values for molecular clouds (see, e.g., Bensch et al. 2001 for a compilation of clouds with indices between 2.5 and 3.3). This implies more structure on smaller scales and thus that the lower column density gas has more structure. This was already pointed out by Falgarone et al. (?) who studied the diffuse component of the interstellar medium, finding highly dynamic and fractal structures.

More examples and a discussion of the values with regard to turbulence models will be given in Sec. 4.2.2.

4.2. Extinction maps

4.2.1. Δ -variance from extinction maps

Figures 3 to 6 show extinction maps of Galactic molecular clouds, obtained with the method described in Appendix B, and the corresponding Δ -variance (for regions where ^{13}CO data was available from the literature, we added these spectra). We determined the Δ -variance without rms-weighting in the IDL routine 'deltavar', using the Mexican-hat filter with a diameter ratio of 1.5, recommended by Ossenkopf, Krips and Stutzki (2008a). All maps are extended and include all major emission regions so that they do not suffer from edge-effects that can disturb the determi-

nation of the Δ -variance (Bensch et al. 2001). However, "empty" regions also contribute to the Δ -variance appearing as large coherent structures so that they produce a decay of σ_Δ^2 at large lags which is shallower than the L^{-2} decay that would represent a zero correlation at those scales (Ossenkopf, Krips, Stutzki 2008a).

The regions that were analysed comprise close-by (distance < 1 kpc), low-mass star forming regions like Perseus, Taurus or the Pipe Nebula, as well as more distant (up to 3 kpc) high-mass star forming regions like Cygnus, Rosette or W3.

A number of spectra show a simple rising curve (e.g. NGC2264, Coalsack, Vela), some including a noise decrease plus a contribution due to empty regions (W3, Taurus, Chameleon). The majority of spectra have more complex shapes, (e.g. Lupus, MonR2, MonOB1, IC 5146, Pipe) with positive or negative curvature and/or two more or less pronounced peaks. Interestingly, the most filamentary structured clouds, partly with very thin, elongated features (Taurus, Chameleon) have the most complex double-peak curves and show low values of β . For these sources, the first peak represents typically the width and the second the length of the filament. However, the shape of the Δ -variance and the value of β weakly depend on the size of the region that is selected. Subregions in a map (e.g. for Vela, where only the high column density region was selected from the A_V map), generally produce slightly steeper spectra with higher values of β . Large maps showing extended filamentary structures produce flatter spectra (e.g. Taurus, Chameleon, Pipe).

4.2.2. Comparison to ^{13}CO data

For regions where we had literature values or own data, we included the Δ -variance determined from ^{13}CO , i.e. Perseus, NGC 2264, Orion A+B, Rosette, Cygnus, and Mon R2. The spectrum of the massive GMCs Cygnus and Rosette look significantly different compared to the spectra derived from the extinction maps. For Cygnus, the curve determined from the A_V -maps represents well a fully self-similar scale distribution, covering all scales (since it is a very large and extended map), while the ^{13}CO spectrum shows the double-peak feature already discussed in Sec. 4.1. There, we attributed the two peaks from the ^{13}CO curve at ~ 4 and ~ 40 pc to the typical filament-sizes in Cygnus X, arising from clouds at a distance of 1.7 kpc and/or optical depths effects of the ^{13}CO line emission. However, these two characteristic scales are not apparent in the Δ -variance spectrum of the extinction map. A possible explanation is that since the A_V map comprises all emission features along the line-of-sight, including the one from the low-density Cygnus Rift in 600 pc distance, the resulting spectrum appears indeed self-similar since it is a composite of diffuse, fractal gas and denser structures. It is thus possible that by using the ^{13}CO line, low density larger scale structures that do not emit in ^{13}CO around $\sim 10' - \sim 100'$ are partly filtered out. However, the two spectra show a similar increase of the Δ -variance (up to a scale of about $10'$) with the slope of the extinction map being slightly shallower. The Rosette spectrum has the same tendency to show a peaked structure in ^{13}CO with a plateau around 8 pc and then a slight decrease, while the extinction map has no characteristic scale. However, for small lags, the spectra show a very different behaviour. Since the ^{13}CO spectrum is not affected by noise for small lags, the spectrum increases in a similar way like for Cygnus (up to $20'$). The spectrum from the A_V -map, on the other hand, is limited by noise for small lags and is thus not directly comparable to the ^{13}CO spectrum. The opposite is true for large lags. The 8

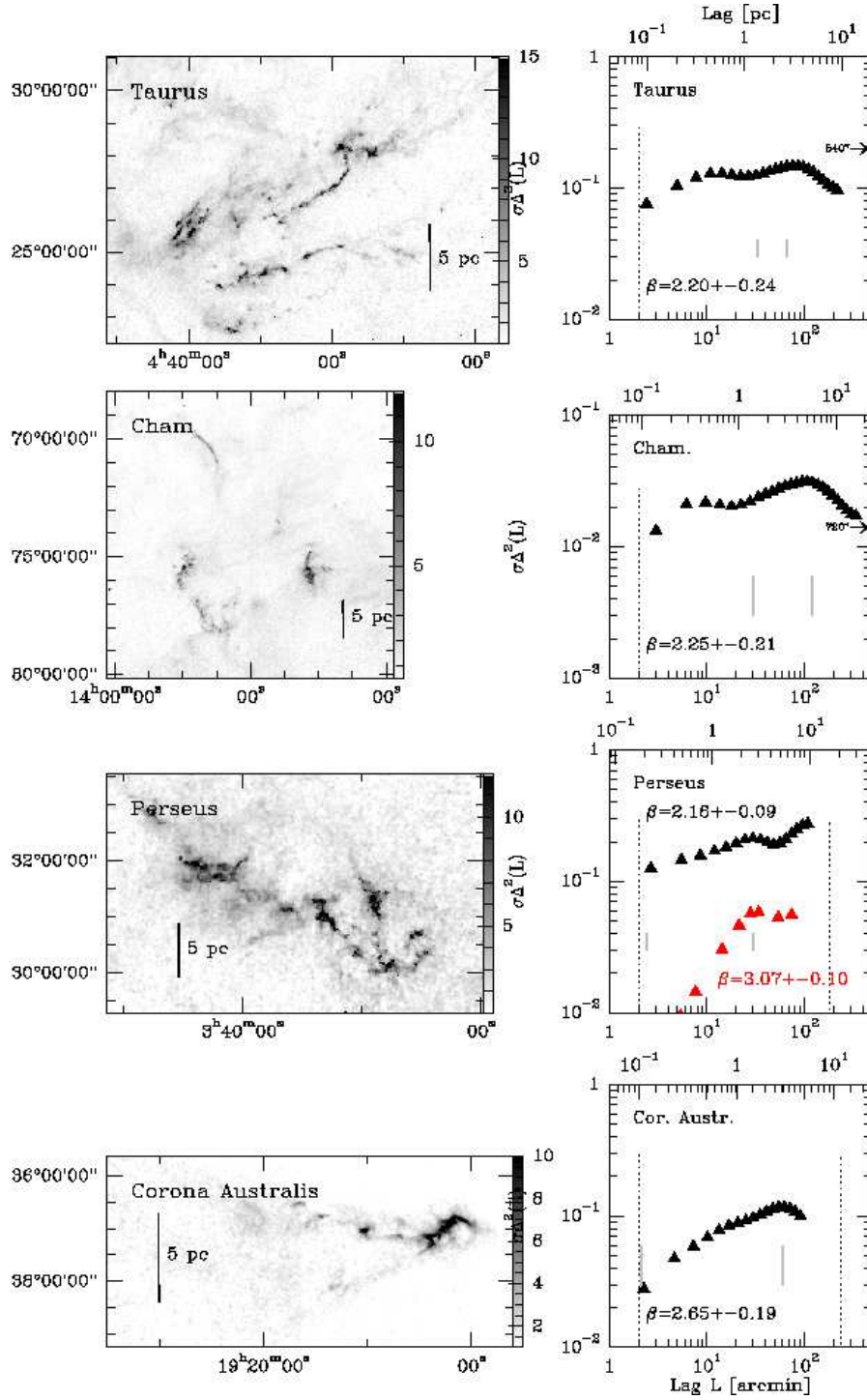


Fig. 3. Extinction maps of Galactic molecular clouds (left) and corresponding Δ -variance spectrum (right). The grey scale range of extinction (A_V) is given in the wedge of each plot. The dashed lines indicate the pixel size (2') and the size of the map. If the mapsize is larger than the x-axis scale (500 arcmin), its size is noted in the plot. The small-scale slope β and its error are given in each diagram, the fit range is indicated by two grey lines. For the sake of clarity, we omitted error bars in the figures. Typical errors are of the order of the ones shown in Fig. 2. The red curve for Perseus represents ^{13}CO 1 \rightarrow 0 data from the Bell Labs (see Table 1 and Bensch et al. 2001). The lower x-axis is labelled in arcmin, the upper one in parsec. All coordinates are in RA and DEC epoch2000.

pc scale may again indicate the scale when the ^{13}CO line becomes optically thick. The larger scale for Rosette compared to Cygnus (4 pc) could be due to the fact that the average density of clumps in Cygnus (Schneider et al. 2006) is higher than in

Rosette (Williams et al. 1995) and thus the ^{13}CO line is saturated on a smaller scale.

For the other sources (Perseus, Orion A/B, Mon R2, and NGC2264), we obtained the Δ -variance from Fig. 10 in Bensch et al. (2001), based on ^{13}CO 1 \rightarrow 0 data from the Bell Labs 7m

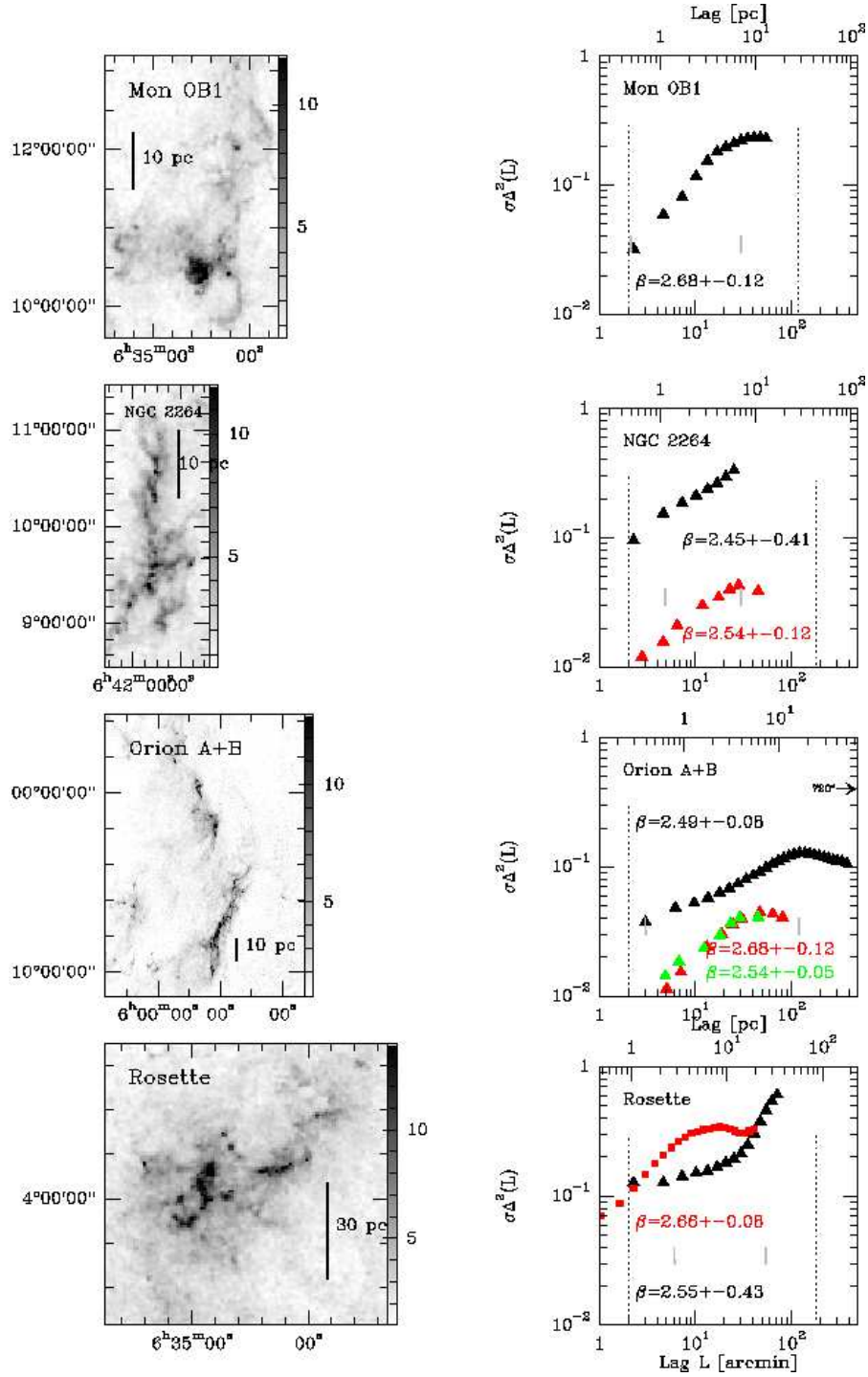


Fig. 4. Extinction maps of Galactic molecular clouds (left) and corresponding Δ -variance (right). See Fig. 3 for further explanations. The red curves for NGC 2264 and Orion B represent ^{13}CO 1 \rightarrow 0 data from Bell Labs (see Table 1 and Bench et al. 2001). The green curve shows the spectrum for Orion A using ^{13}CO 1 \rightarrow 0 data from Bell Labs. The red curve for Rosette stems from ^{13}CO 1 \rightarrow 0 data from FCRAO (Heyer, Williams, Brunt 2006).

telescope survey (Bally et al., priv. communication). The form of the spectrum is rather similar to the ones obtained from the A_V -maps but the location of peaks and the values of β slightly differ. It seems that the angular resolution of the maps has an influence on the shape of the Δ -variance since its form for the extinction maps (at 2' resolution) correspond well to the 1.7' Bell Labs data but differ from that of the 50'' resolution FCRAO surveys. A recent study of Brunt (2010, submitted to A&A) of

Taurus, comparing the power spectra determined from ^{13}CO and A_V showed that they are almost identical.

4.2.3. The Δ -variance for all clouds

Figure 7 shows the Δ -variance spectra for all clouds in this study obtained from the A_V -maps. At small scales (below 1 pc) most sources show a non-constant spectral index steepen-

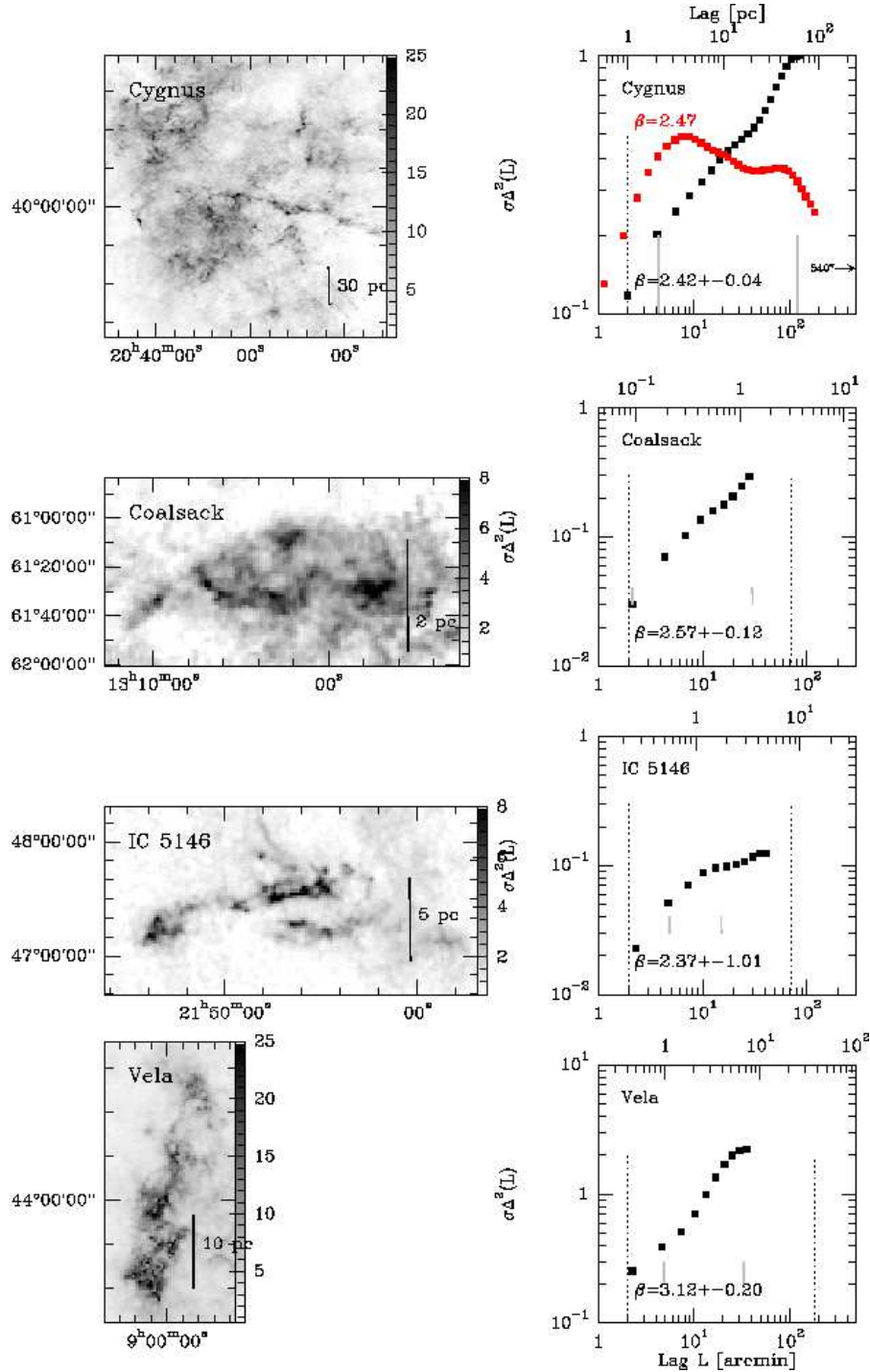


Fig. 5. Extinction maps of Galactic molecular clouds (left) and corresponding Δ -variance (right). The red curve for Cygnus represents the ^{13}CO 1 \rightarrow 0 data from the FCRAO survey. See Fig. 3 for further explanations.

ing towards the lowest scales. This is consistent with decaying turbulence dissipated at small scales (Ossenkopf & Mac Low 2002) but also with driven turbulence at small lags (Federrath et al. 2009). However, there are three exceptions: Chameleon and Taurus show an intermediate peak at 0.3–0.4 pc and Perseus shows no clear indication of a steepening. The intermediate peak might mean that the extinction map is affected by a separate, more distant, component that is actually dominated by structures larger than assigned in the plot (see also discussion below). Alternatively, it could be produced by a systematic structure of the detected size that affects the turbulence in the cloud.

Candidates for such structures are SN-shells. Expanding ionization fronts from OB associations also impact on the cloud structure. For example, it is known that Lupus is influenced by a subgroup of the Sco OB2 association (Tachihara et al. 2001) both by past SN explosions and present OB stars. Cygnus is exposed to the very massive OB2 cluster (Knödseder et al. 2000) but lacks SN shells. Orion A and B are influenced by stellar wind driven compression centered on Ori OB 1b.

Around a size scale of 1 pc, we typically find a self-similar scaling regime. The slope of the Δ -variance spectrum there reflects the filamentary structure of the source. The one extreme is

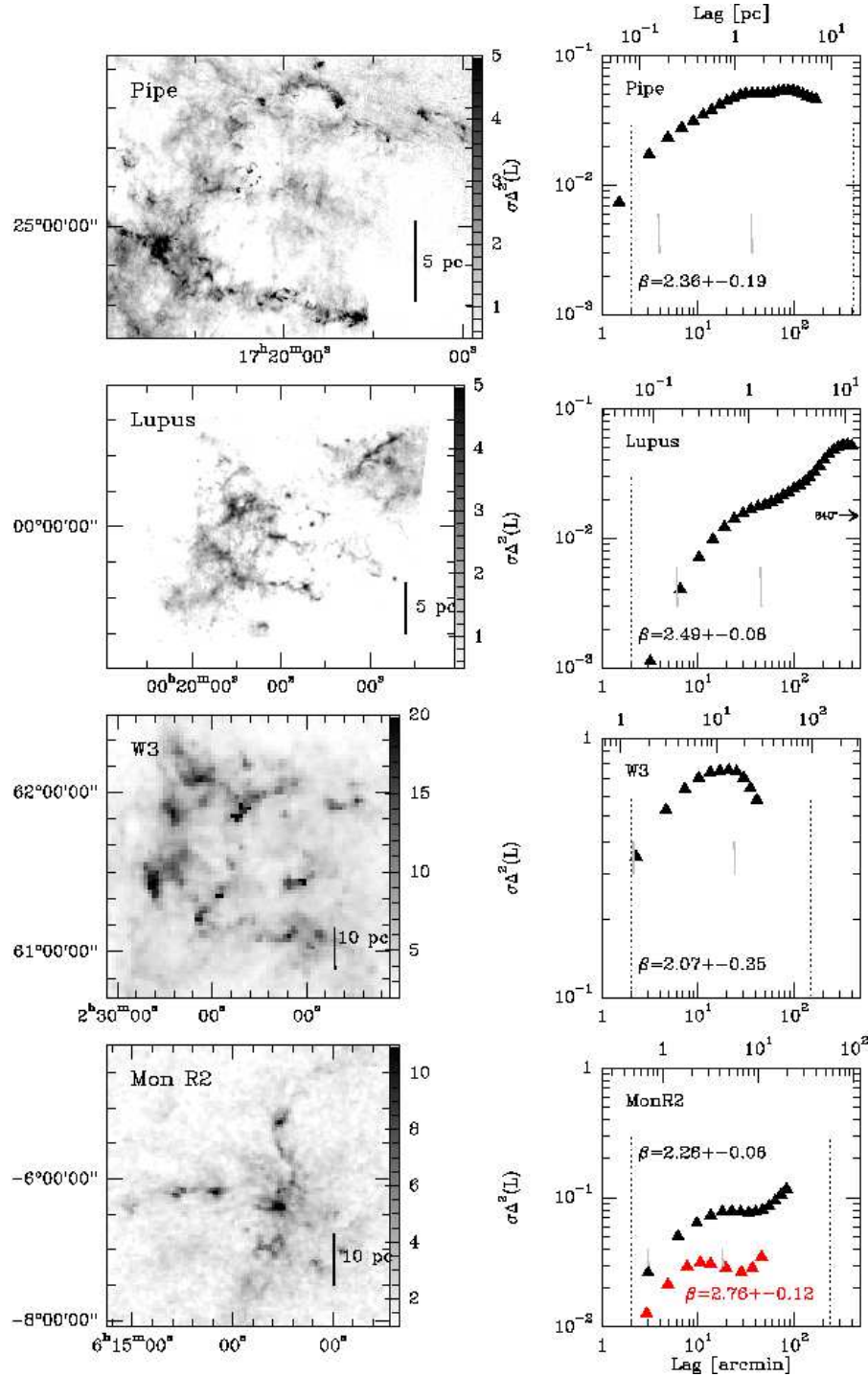


Fig. 6. Extinction maps of Galactic molecular clouds (left) and corresponding Δ -variance (right). The red curve for MonR2 represents data from a ^{13}CO 1 \rightarrow 0 Bell Labs survey (see Table 1 and Bench et al. 2001). See Fig. 3 for further explanations.

formed by the extremely filamentary Perseus cloud with a very shallow spectrum. The other one by Mon OB1 which is very condensed leading to a steep spectrum.

At scales above 1 pc nearly all low-mass SF clouds show a characteristic size scale as a peak of the Δ -variance spectrum (see Sec. 4.2.4), i.e. Cor. Australis, Taurus, Perseus, Chameleon, Pipe) show a common peak scale at 2.5–4.5 pc. This indicates the scale of the physical process governing the structure formation. This could e.g. be the scale at which a large-scale SN shock sweeping through the diffuse medium is broken at

dense clouds, turning the systematic velocity into turbulence. The GMCs, on the other hand, show no break of the self-similar behavior at all up to the largest scales mapped. The Rosette is completely dominated by structure sizes close to the map size. At the largest, Galactic scales, energy injection due to, e.g., spiral density waves should be visible on a kpc size, well above our limits.

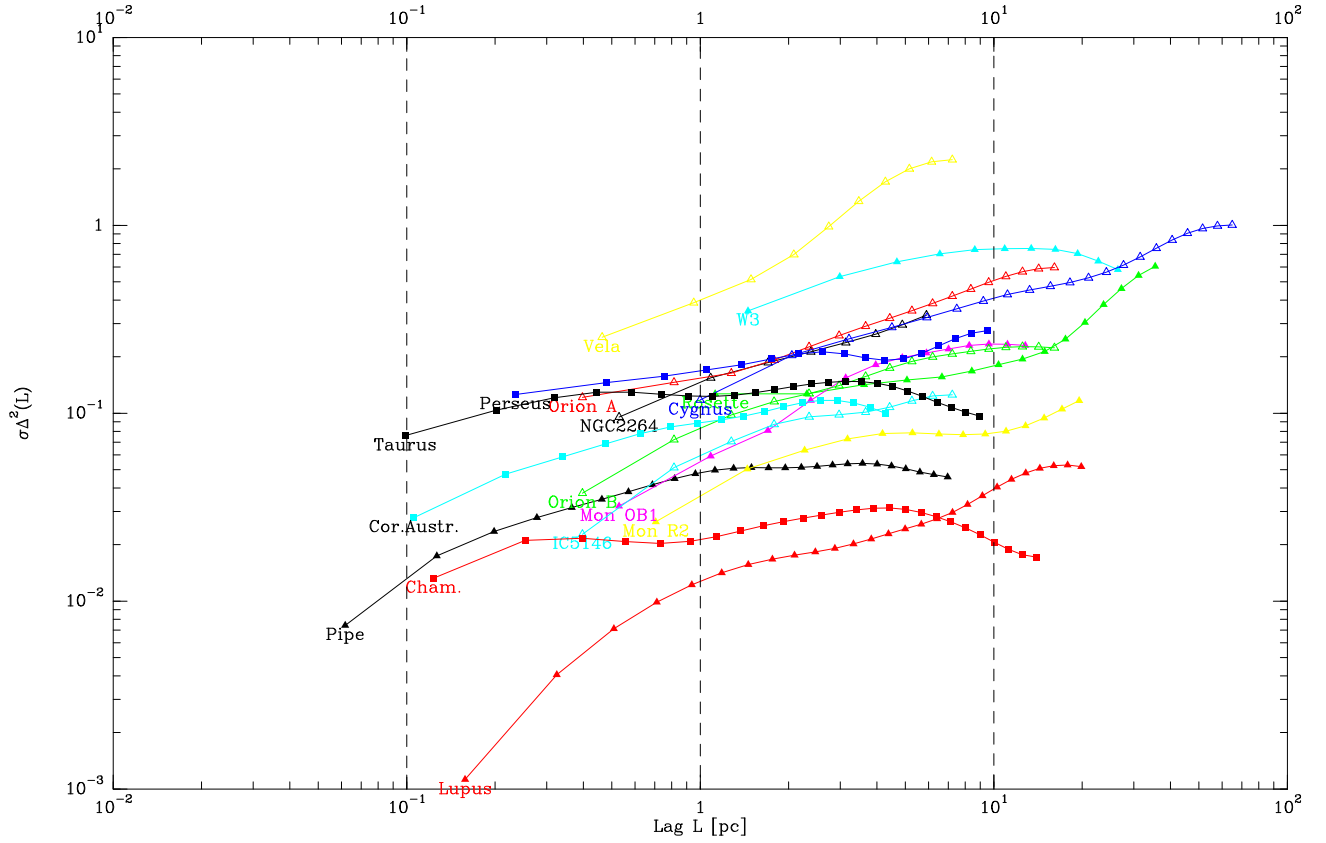


Fig. 7. Δ -variance spectra of all sources where we obtained A_V maps in this study. The Lag scale is in parsec.

4.2.4. Are there characteristic size scales depending on the type of cloud ?

Although the Δ -variance determined from extinction maps shows interesting particularities for different clouds, one has to note that there can be large differences in the value of β within each individual complex, as was shown by Sun et al. (2006) for Perseus. We thus have to be careful in interpreting different values of β and the shape of the spectrum depending on the type of cloud and tracer. In Table 1, we listed β for different gas phases, from diffuse HI gas to low-and high-mass star forming regions, obtained from maps with different tracers (HI, isotopomeric CO lines, extinction maps and dust continuum). In total, the values range from 2.07 (W3) to 3.12 (Vela) and are thus in the typical range of values determined for other studies (e.g. Bensc et al. 2001). However, if we exclude the most extreme data points for W3 and Vela and the very disperse results for Perseus, the range of β -values is much more narrow, only 2.16 to 2.76. But in any case, no systematic trend can be seen between the value of β and the type of cloud/gas phase. However, all β values determined from ^{13}CO are systematically higher than the ones obtained from the extinction maps. In addition, based only on ^{13}CO data, there is a slight tendency that high-mass SF regions have lower values of β than low-mass SF regions. We do not see a trend with distance (since shorter distances to a cloud resolve smaller scale structures and thus β should be higher).

We also tried to see a characteristic scale in the spectra with one or two peaks, i.e. we listed in Table 1 the parsec-scale where a first and possible second peak were observed. Interestingly, all clouds that show a double-peak structure are low-mass SF regions in galactic regions that are not (much) affected by line-of-sight crowding. The more massive and denser high-mass star

forming clouds show no clear double-peak structure. This can partly be due to the fact that most of them are further away (W3, Cygnus, Rosette are all at distances >1.5 kpc) and thus the extinction maps are sensitive for all gas along the line-of-sight and therefore to all structure scales. However, other massive clouds like NGC2264, the Orion clouds and Vela are closer (<1 kpc) and do not show a double-peak structure either. The first peak for low-mass SF clouds occurs at size scales that are characteristic for molecular clumps, i.e. 0.4 to 1.5 pc (with one higher value for Perseus of 2.5 pc). The second peak is found between 2.9 and 4.6 pc. Blitz & Williams (1997) found a characteristic size scale of 0.25–0.5 pc indicating a change in structure in Taurus, conform with our finding for Taurus. A small sample of clouds (Orion A, ρ Oph, Taurus, and L1512) was investigated by Falgarone et al. (2004) using ^{13}CO 1 \rightarrow 0 emission. They found a typical size scale of around 0.5 pc for the width and 1 to 18 pc for the lengths of filaments. Our sample is more homogeneous in its values and we may trace here two different physical processes, one leading to the formation of clumps (1 pc scale) and one to the formation of filamentary structures (4 pc scale as the lengths of the filaments). However, the typical width of filaments is around 1 pc as well which complicates the picture. These scales may thus be associated with turbulence driven on small scales and turbulence driven on larger scales. This is an interesting result since the physical properties and the driving vary from cloud to cloud. It might be, for example, that energy injection from outflows is more important for Perseus than for Taurus (the latter contains much less sources) and thus leads to a slightly different characteristic scale since turbulence driven by outflows acts on smaller scales than turbulence driven by large scale events like SN explosions. The picture might be different for massive GMCs that show no characteristic scales in A_V maps and none in ^{13}CO

Table 1. Observed values of the power-law exponent β (column 4) in different phases of the ISM (from diffuse HI gas to GMCs). Values for β obtained from our extinction maps are indicated in bold. Column 5 and 6 indicate the size scale in parsec where spectra show peak values. Values in parenthesis are less reliable, the spectrum shows not a prominent peak there. Values given only for peak 2 indicate that there is only one prominent peak. Note that for Orion, we determined β individually for the subregions Orion A and B (for direct comparison to the ^{13}CO data) and for the whole complex, which is also shown in Fig. 4.

Region	Distance [pc]	Tracer	β	peak 1 [pc]	peak 2 [pc]	Reference
Diffuse HI		HI	2.6–2.8			Green et al. (1993)
North Polar Spur		HI	3.6			Miville-Deschenes (2003)
Diffuse Clouds						
Polaris Flare	150	$^{13}\text{CO } 1\rightarrow 0$	2.77			Stutzki et al. (1998)
Polaris Flare		$^{13}\text{CO } 2\rightarrow 1$	2.76			Falgarone et al. (1998), Stutzki et al. (1998)
low-mass SF cloud						
Perseus	300	$^{13}\text{CO } 1\rightarrow 0$	3.07	2.7	(>10)	Bensch et al.(2001)
Perseus		$^{13}\text{CO } 1\rightarrow 0$	3.09			Sun et al.(2006)
Perseus		$^{13}\text{CO } 2\rightarrow 1$	3.03			Sun et al.(2006)
Perseus		$^{12}\text{CO } 1\rightarrow 0$	3.08			Sun et al.(2006)
Perseus		$^{12}\text{CO } 3\rightarrow 2$	3.15			Sun et al.(2006)
Perseus		extinction	2.55			Sun et al.(2006)
Perseus		extinction	2.16	2.5	(>10)	
Taurus	140	extinction	2.20	0.5	3.5	
Chameleon	160	extinction	2.25	0.4	4.6	
Pipe Nebula	140	extinction	2.36	1.5	3.8	
IC 5146	400	extinction	2.37	(1.4)	(>4.5)	
Lupus	100	extinction	2.49	(1.5)	(>10)	
Coalsack	150	extinction	2.57	-	-	
Corona Australis	170	extinction	2.65	-	2.9	
GMC						
W3	2200	extinction	2.07	-	11	
Cygnus	1700	$^{13}\text{CO } 1\rightarrow 0$	2.47	4	40	this study
Cygnus		extinction	2.42	-	-	
Orion A	450	$^{13}\text{CO } 1\rightarrow 0$	2.54	-	6	Bensch et al. (2001)
Orion A		extinction	2.49	-	-	
Orion B	450	$^{13}\text{CO } 1\rightarrow 0$	2.68	-	6	Bensch et al. (2001)
Orion B		extinction	2.40	-	>13	
Orion A+B		extinction	2.49	-	17	
Mon R2	800	$^{13}\text{CO } 1\rightarrow 0$	2.76	2.75	>11	Bensch et al. (2001)
Mon R2		extinction	2.26	3.9	>20	
Mon OB1	800	extinction	2.55	(4)	>10	
Rosette	1600	$^{13}\text{CO } 1\rightarrow 0$	2.66	-	>7.5	Heyer et al. (2006)
Rosette		extinction	2.55	-	-	
NGC 2264	800	$^{13}\text{CO } 1\rightarrow 0$	2.54	-	6.7	Bensch et al. (2001)
NGC 2264		extinction	2.45	-	-	
Vela	700	extinction	3.12	-	>7	

maps, if we assume that the characteristic scales around a few parsec arise from optical depths effects. Heyer & Brunt (2006) for example found no difference in the scaling coefficient for the velocity structure function (see, e.g., Brunt 2003 for details) for the Rosette Molecular Cloud, a GMC forming actively massive stars and strongly influenced by an expanding HII region, and G216-2.5, an even more massive cloud but with very little low-mass SF. They conclude that energy input at large scales sustains the global turbulence in molecular clouds while effects like expanding HII regions or outflows act locally in modifying the turbulent structure.

It should also be noted that our resolution is not high enough to resolve molecular cores. Their typical size is 0.1 pc (e.g., Motte et al. 2007) and we are well above this limit. It would be interesting to apply the Δ -variance on large maps at high angular resolution to resolve cores, clump and filaments at the same time.

4.3. Δ -variance and turbulence models

A comparison between turbulence models and observations is required in order to understand the processes that govern the structure of the cloud. Models with different parameters (purely hydrodynamic or with magnetic field, with or without self-gravity, driven or decaying turbulence etc.) will produce different Δ -variance spectra that can be compared to observations. The Δ -variance was used by Mac Low & Ossenkopf (2000) to characterize the density and the velocity structure of interstellar turbulence simulations. They found that only driven, supersonic hydrodynamical turbulence (with or without magnetic fields) can maintain self-similar, power-law behaviour at scales less than the driving scale. Ossenkopf, Krips & Stutzki (2008b) showed that energy injection on a particular scale does not create density enhancements on that scale but on one which is 20% to 25% smaller. The slopes of the Δ -variance for these models is in the range of values typically observed for molecular clouds (≈ 2.3 – 3.1 , see Table 4.2.3). On the other hand, slow, decaying

turbulence provokes characteristic length scales. Our observations are conform with the driven turbulence model, though these do not include self-gravity and radiative transfer (which need to be considered to give a more realistic scenario). Ossenkopf, Klessen and Heitsch (2001) included self-gravity in their hydrodynamic models and showed that collapsing cores within a molecular cloud produce small scale structures that dominate the density structure, and thus produce a *negative* slope in the Δ -variance spectrum. This effect is probably only visible when using optically thin tracers sensitive for dense gas (Ossenkopf 2002), which is not the case of our extinction maps. However, a first try performed by Ossenkopf, Krips and Stutzki (2008b) using a large mm-continuum map in ρ Oph (Motte et al. 1998) did not show a negative slope but the typical shape of the Δ -variance observed in molecular clouds.

A recent application of the Δ -variance on model simulations was performed by Federrath, Klessen & Schmidt (2009). They used the Δ -variance to characterize the density structure produced in supersonic, isothermal hydrodynamic models with two limiting cases of turbulence forcing: solenoidal (divergence-free) vs. compressive (curl-free) forcing. Table 2 shows that the compressive forcing models produce systematically higher values of β than the solenoidal ones. All values are, however, at the upper limit of the range typically obtained from molecular cloud studies. Interestingly, a high value of β is better consistent with the Δ -variance spectra determined from diffuse Galactic HI emission (see Table 1), and seems consistent with Kolmogorov scaling of incompressible turbulence (Falgaron et al. 2004). The transition to incompressible turbulence, however, is expected to occur close to the sonic scale at about 0.1 pc (Federrath et al. 2009). Scales larger than that are clearly in the supersonic regime. The steepening of the power-law index β towards large scales in HI clouds and in the numerical model with compressive forcing is thus unlikely to represent incompressible turbulence. It is more likely that the cloud-like structures on intermediate scales (see Fig. 1, right panel in Federrath et al. 2009) produce a relative steepening of the spectral index on large scales. A similar effect might occur for dense molecular cloud structures embedded in the diffuse atomic HI gas. In contrast, the steepening of β on scales smaller than 0.1 pc (see Bensch et al. 2001) indicates a transition to coherent cores (Goodman et al. 1998) with transonic to subsonic, almost incompressible turbulence, because this transition is likely to occur close to the sonic scale.

Table 2. Values of β from hydrodynamic simulations of supersonic, isothermal turbulence with solenoidal (divergence-free) and compressive (curl-free) forcing (Federrath et al. 2009).

	Forcing	β
3d-hydrodynamic simulation	solenoidal	2.89
3d-hydrodynamic simulation	compressive	3.44
2d-projection	solenoidal	2.81
2d-projection	compressive	3.37

5. Summary

We presented a 35 square degrees $^{13}\text{CO } 1\rightarrow 0$ molecular line survey of Cygnus X, taken with the FCRAO, and visual extinction (A_V) maps of 17 Galactic clouds, obtained from near-IR 2MASS

data, in order to analyse the spatial structure of molecular clouds using the Δ -variance method.

For Cygnus, we found no characteristic scale in the A_V -map but a double-peak spectrum for the Δ -variance from ^{13}CO with peaks at 4 pc and 40 pc. The 4 pc scale corresponds to the typical size scale found for low-mass star-forming nearby clouds (see below), characterizing a typical small filament size, while the second peak around 40 pc arises from the largest filamentary structures seen in Cygnus. This scale is larger than the whole extent of the cloud (~ 100 pc). An alternative explanation is that the 4 pc scale is the characteristic scale when the $^{13}\text{CO } 1\rightarrow 0$ line becomes optically thick. Generally, ^{13}CO observations may provide only a good reflection of the structure measured up to about $A_V=5^m$. The exact location of the peaks on the Delta-variance spectrum gives some measure for the turbulence in the molecular cloud. They indicate a transition from more coherent structures, where the ^{13}CO emission falls into a narrow velocity interval, to a wide-spread turbulent distribution leading to a dilution of the optical depth in very broad lines. The origin of energy injection in Cygnus can be manifold. It is known that the region is strongly affected by radiation from the Cygnus OB2/OB9 clusters, expanding HII regions, and a large number of outflow sources. However, no signatures of supernova-shells were yet found in Cygnus X, seen as one of the most important energy source (MacLow & Klessen 2004). The power spectral index β , determined from the Delta-variance spectrum $\sigma_\Delta^2 \propto L^{\beta-2}$ with the size parameter L , has a value of $\beta=2.53$ which is at the lower end of typical values for molecular clouds (typically between 2.5 and 3.3).

The Δ -variance spectra obtained from the A_V maps show differences between low-mass star forming (SF) clouds and massive giant molecular clouds (GMC) in terms of shape of the spectrum and values of the slope β . Many of the low-mass SF clouds have a double-peak structure with characteristic size scales around 1 pc and 4 pc. These scales may represent SF molecular clumps (1 pc) and/or the width (1 pc) and length (4 pc) of filaments or the overall cloud size. The physical process governing the structure formation could be the scale at which a large-scale SN shock sweeping through the diffuse medium is broken at dense clouds, turning the systematic velocity into turbulence. GMCs show no characteristic scale in the A_V -maps which can partly be ascribed to a distance effect due to a larger line-of-sight (LOS) confusion. The values of β show no clear trends, there is a tendency that all β values determined from ^{13}CO are systematically higher than the ones obtained from the extinction maps and that high-mass SF regions have lower values of β than low-mass SF regions. We do not see a trend with distance (since shorter distances to a cloud resolve smaller scale structures and thus β should be higher).

A comparison between the Δ -variance determined from model simulations (supersonic, isothermal hydrodynamic models with solenoidal (divergence-free) vs. compressive (curl-free) forcing, Federrath, Klessen & Schmidt (2009)) and observations shows that the model values are systematically higher.

Acknowledgements. We thank M. Heyer and J. Williams for providing us with the $^{13}\text{CO } 1\rightarrow 0$ FCRAO data from the Rosette Molecular Cloud.

Appendix A: Data quality

The data points of the surveys were irregularly sampled and thus regridded to a fully sampled $22''.5$ grid. The aliased noise power was minimized and the full resolution of the telescope retained. The convolution kernel used was

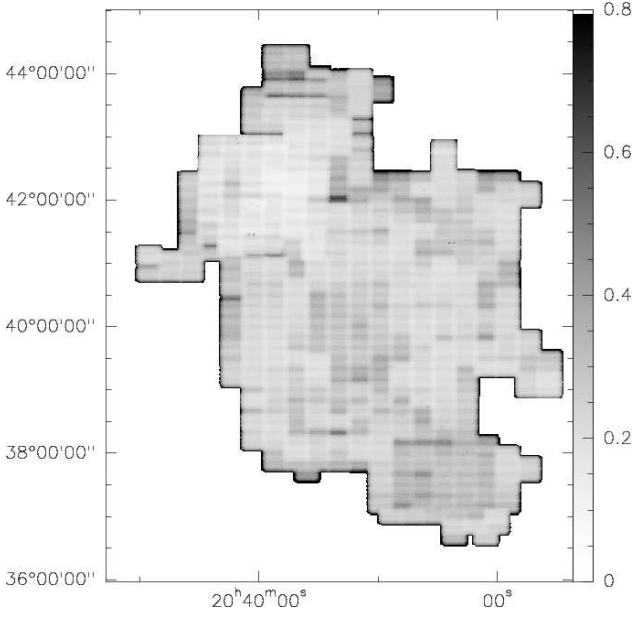


Fig. A.1. Rms map of the ^{13}CO (C^{18}O) data in K.

$$\frac{J_1(2\pi ax)}{2\pi ax} \frac{J_1(cx/R_{\max})}{cx/R_{\max}} e^{-(2bx)^2} \Pi(R_{\max})$$

with J_1 the first-order Bessel function, x the distance from the observed data point, R_{\max} the truncation radius ($R_{\max}=3$), $a = 0.9009$, $b = 0.21505$, and $c = 3.831706$. $\Pi(R_{\max})$ is used as a pill box function with $\Pi = 1$ for $R < R_{\max}$ and $\Pi = 0$ for $R > R_{\max}$.

The gridded spectra were converted and stored in CLASS spectra files. CLASS is a part of the GILDAS package and was used to further reduce the data. The data for small regions, typically $30' \times 30'$, were reduced in a data reduction pipeline. First, all spectra in the region were averaged to determine the window around the emission to be excluded from the baseline fit. Second, a first to third order baseline was subtracted from all spectra. The reduced spectra were then written to 3-d data cubes (RA, DEC, velocity). Afterwards, cubes of the individual regions were merged to a single 3-d data cube for application of the Δ -variance.

In order to quantify the quality of the survey, we produced rms noise maps of all line tracers, the one of ^{13}CO is shown in Fig. A.1. It becomes obvious that the noise is not uniform but shows a checkerboard structure and the edges are more noisy than the center. Both effects are due to the observing mode. In the OTF mode, a single position is passed by several pixels of the receiver array, resulting in a dense sampling and thus, an improved signal-to-noise ratio in the inner regions of an OTF map. Towards the map edges, the sampling is not as dense causing higher rms values. Since the individual maps were observed with overlap to assemble the final large scale data set, the overlap regions are sampled a little more densely. The lower rms values in these overlaps create the checkerboard structure. The plot also highlights the areas which have been observed twice, namely the DR21 region.

Appendix B: Extinction maps from dust reddening of 2MASS sources: the example of Cygnus X

The main purpose of developing AvMAP instead of using other programs (e.g. NICER; Lombardi et al. 2001) is that it can han-

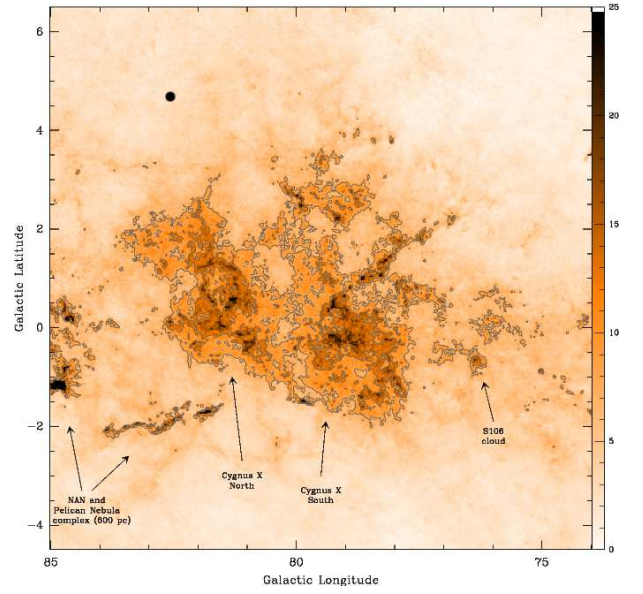


Fig. B.1. Map of the extinction (A_V) toward the Cygnus X region obtained from the reddening of 2MASS point sources. The A_V derivation is optimized for a distance of 1.7 kpc, and is over-estimated for the more nearby complex of the North America and Pelican Nebulae. The Cygnus X complex is well visible and appears as mostly two large complexes referred to in Schneider et al. (2006) as Cygnus X North and South. One can also note that the S106 cloud is well visible in the southern part of Cygnus X.

dle foreground stars up to larger distances and without assumptions or off-field evaluation of the density of these foreground stars. Like that, we are able to image the most distant clouds. To illustrate our technique of deriving extinction maps from near-IR 2MASS data we describe in detail, as an example, the case of Cygnus X.

The resulting A_V map for a field of $10^\circ \times 10^\circ$ toward Cygnus X is displayed in Figure B.1. In this large field, a total of 4.5×10^6 stars is found with an average of 12.4 stars per arcmin². The individual A_V are measured as the quadratic, uncertainty weighted average of the two A_V estimates obtained from the two 2MASS colors [J–H] and [H–K]. The individual uncertainties are given by the quadratic sum of photometric uncertainties (from the catalog) and of the uncertainties on the intrinsic colors of a typical Galactic star (see for instance Lombardi et al. 2001 2001 for more details). The adopted values are $[J-H]_0 = 0.45 \pm 0.15$, and $[H-K]_0 = 0.12 \pm 0.05$ with the associated uncertainties measured from the color dispersions for a population of Galactic stars as measured using simulations with the Besançon Galactic models (Robin et al. 2003; see below).

B.1. Prediction of the density of foreground stars

The above described method to estimate dust column densities entirely relies on the hypothesis that the near-IR sources are background stars. However, for a distant region like Cygnus X, a significant density of foreground stars is expected. To properly measure the dust column density, the foreground stars have to be filtered out (see detailed discussion in Cambresy et al. 2002).

We use the predictions of the Besançon stellar models to derive a systematic, independent estimate of the expected number of foreground (n_{fg}) stars for any Galactic direction. Catalogs of sources have been simulated using the online sim-

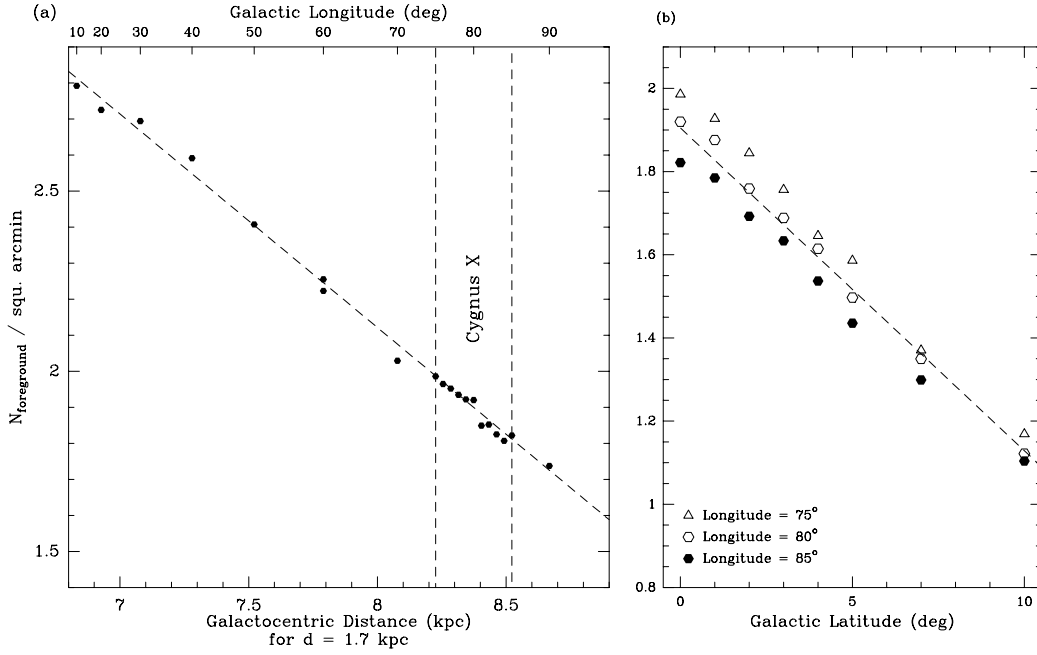


Fig. B.2. Variation of n_{fg} measured from simulations using the Besançon model (see text) (a) in the Galactic plane as a function of longitude; and (b) in the Cygnus X region as a function of latitude. The variation with longitude is actually expressed as a function with r_{GC} (see text). These predicted foreground star densities have been derived for a distance from Sun of 1.7 kpc. The adopted linear interpolations are displayed as dashed lines.

ulator (<http://model.obs-besancon.fr/>) for a list of representative Galactic directions. For each simulated catalog, the number of stars brighter than the 2MASS completeness levels for all filters ($J=17.0$, $H=16.5$ and $K=16.0$), and at a distance smaller than the cloud distance ($d = 1.7$ kpc) is calculated to derive the expected density of foreground stars. Figure B.2 displays the resulting values of n_{fg} for 20 positions on the Galactic plane ($lat=0$) from $lon=10$ to 90° , and for 21 other positions at three fixed longitudes ($lat=75^\circ$, 80 and 85°) from $lat=0$ to 10° . Note that n_{fg} is expressed as a function of the Galactocentric distance r_{GC} (down axis) using $R_\odot = 8.5$ kpc. The Cygnus X region corresponds to r_{GC} between 8.22 and 8.52 kpc where n_{fg} is decreasing from ~ 2 to 1.8 star per arcmin², which is of the order of 10 % of the average density of 2MASS sources. The effect of latitude is larger with a typical decrease from ~ 1.9 to 1.1 star per arcmin² for $lat=10^\circ$. In order to filter out foreground stars, we then assumed that they are always the bluest stars in each direction which might not be always fully correct for the lowest extinction regions.

B.2. Distribution of young stars

Young stars are usually more luminous than the population of background stars. If they are low or intermediate mass young stars, they are still above the main sequence, and if they are massive, they are luminous and necessary young due to their fast stellar evolution. In the 2MASS catalog, these young stars are not necessary brighter than the surroundings due to the flux attenuation (extinction) of the parental cloud. However, following the same idea like to derive the average total extinction, the fluxes of all 2MASS sources can be de-reddened to evaluate their intrinsic brightness. Since the young stars form in clusters, maps of the distribution of the brightest IR sources after dereddening should trace well the embedded clusters. We thus use the

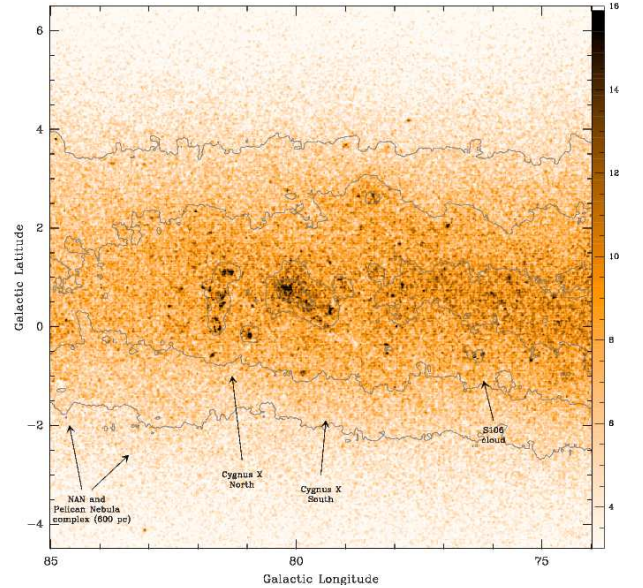


Fig. B.3. Map of the source density with a dereddened K band ($2\mu m$) magnitude smaller than 13. The linear scale is given as a slider on the right and is expressed in number of sources per arcmin². The Cyg-OB2 association in the middle is clearly visible (see also Knödlseider (2000)). A number of embedded clusters inside Cygnus X North could be the seeds for a newly formed OB association.

same A_V -mapping procedure to produce at the same time density maps of the brightest dereddened stars. For the flux cut to be used, a good compromise between the 2MASS sensitivity and the typical brightness of young stars has been found to be between $K=12$ and $K=13$. With a cut at $K=12$ a large number of cluster members can be found. In contrast, a cut at $K=13$ is more

selective and can secure the detection of a cluster difficult to recognize.

Figure B.3 below displays the map of the density of stars with $K > 13$ in the Cygnus X region after dereddening. It clearly shows a large-scale distribution of stars in the Galactic plane with several extended, higher concentration of stars. On the top of this large-scale distribution a number of small-scale clusters are apparent. A fraction of these clusters were also recognized by eye inspection of the 2MASS images by Dutra&Bica (2001), and using a simplified version of the present imaging procedure by LeDuigou (2002).

B.3. "AvMAP", the fortran implementation of the method

In practice here for the Cygnus X field displayed in Fig. B.1 and B.3, the visual extinction A_V has been evaluated by averaging individual A_V for stars inside gaussian beams for each position in the map and after excluding the required number of probable foreground sources. We adopted a grid of 450×450 pixels with $80''$ spacing, and a resulting gaussian resolution of $1.9'$ (Nyquist sampling). The typical number of 2MASS sources per beam varies typically from 15 to 25 but goes down to close to 10 in regions of high extinctions, and can even reach the typical number of foreground sources (4 to 5 per beam) for the darkest regions. This is particularly the case for the region at $lon \sim 84.7^\circ$ which corresponds to the North America and Pelican Nebulae which are known to be at a distance of only 800 pc and for which, therefore, the number of foreground stars removed is too large leading to an over-estimate of A_V .

In order to compute the different steps to derive A_V and the density of young stars in each pixel of large maps, we coded a FORTRAN90 program with an inner algorithm that is optimized to reduce the number of accesses to the (large) catalog of sources. In fact, for any large map, several millions of stars have to be processed with their coordinates, fluxes and uncertainties. It is impossible to go through millions of sources for each pixel when typically 10^5 pixels are required to image the field. Instead, for each step of the calculation, each source is read only one time, and it is the contribution of this source to the final result which is calculated. Altogether, 3 paths/steps are required to compute A_V and the density of sources n_K .

The most recent version of AvMAP produces images directly in FITS format using the astrolib package. The best supported projection method is gnomonic even if some others implemented projection may work fine too (less tested).

References

- Allan, D.W., 1966, Proc. IEEE, Vol.54, No.2, 221
 Ballesteros-Paredes, J., Mac Low, M.-M., 2002, ApJ, 570, 734
 Bate, M., 2009, MNRAS, 392, 1363
 Bensch, F., Stutzki, J., Ossenkopf, V., 2001, A&A, 266, 636
 Blitz, L., Williams, J.P., 1997, ApJ, 488, L145
 Bonnell, I.A., Dobbs, C.L., Robitaille, et al., 2006, MNRAS, 365, 37
 Brunt, C.M., 2003, ApJ, 582, 280
 Brunt, C.M., Heyer, M.H., Mac Low, M.-M., 2009, A&A submitted
 Cambr  sy, L., Beichman, C. A., Jarrett, T. H., Cutri, R. M., 2002, Astronomical Journal, 123, 2559
 Clark, P.C., Bonnell, I.A., 2006, MNRAS, 368, 1787
 Dib, S., Brandenburg, A., Kim, J., et al., 2008, ApJ 678, 105
 Dib, S., Walcher, J.C., Heyer, M., et al., 2009, MNRAS, 398, 1201
 Dickel, H.R., Wendker, H.J., & Bierritz, J.H., 1969, A&A, 1, 270
 Dutra, C.M., Bica, E., 2001, A&A, 376, 434
 Elmegreen, B., Falgarone, E., 1996, ApJ, 471, 816
 Erickson, N.R., Grosslein, R.M., Erickson, R.B., & Weinreb, S., 1999, IEEE, 47, 2212
 Falgarone, E., Philipps, T., G., Walker, C.K., 1991, ApJ, 378, 186
 Falgarone, E., Hily-Blant, P., Levrier, F., 2004, Astrophysics and Space Science, 292, 89
 Federrath, C., Klessen, R.S., Schmidt, W., 2009, ApJ, 692, 364
 Goldsmith, P.F., Snell, R.L., Hasegawa, T., Ukita, N., 1987, ApJ 314, 525
 Goodman, A.A., Barranco, J.A., Wilner, D.J., et al., 1998, ApJ, 504, 223
 Heitsch, F., Hartmann, L.W., Slyz, A.D. et al., 2008, ApJ 674, 316
 Hennebelle, P., Audit, E., 2007, A&A, 465, 431
 Hennebelle, P., Audit, Miville-Deschenes, 2007, A&A, 465, 445
 Heyer, M., Schloerb, 1997, ApJ, 475, 173
 Heyer, M., Brunt, C., 2004, ApJ, 615, L45
 Heyer, M.H., Williams, J.P., Brunt, C.M., 2006, ApJ, 643, 956
 Kn  dlseder, J., 2000, A&A, 360, 539
 Kolmogorov, A., 1941, Dokl. Akad. Nauk SSSR, vol.30, p.301-305
 Kramer, C., Stutzki, J., R  hrig, R., Corneliussen, U., 1998, A&A, 329, 249
 Lada, C. J., Lada, E. A., Clemens, D. P., Bally, J., 1994, ApJ, 429, 694
 Larson, R.B., 1981, MNRAS, 194, 806
 LeDuigou, J.-M., & Kn  dlseder, J., 2002, A&A, 392, 869
 Lombardi, M., Alves, J., 2001, A&A, 377, 1023
 Loren, R.B., 1989, ApJ, 338, 902
 Mac Low, M.-M., Ossenkopf, V., 2000, A&A, 353, 339
 Mac Low, M.-M., Klessen, R., 2004, Reviews of Modern Physics, vol.76, Issue 1, 125-194
 Miville-Deschenes, Joncas, G., Falgarone, E., Boulanger, F., 2003, A&A
 Motte, F., Andr  , P., Neri, R., 1998, A&A, 336, 150
 Motte, F., Bontemps, S., Schilke P., Schneider, N., Menten, K., 2007, A&A, 476, 1243
 Ossenkopf, V., Klessen, R., Heitsch, F., 2001, A&A, 379, 1005
 Ossenkopf, V., 2002, A&A, 391, 295
 Ossenkopf, V., & Mac Low, M.-M., 2002, 390, 307
 Ossenkopf, V., Krips, M., Stutzki, J., 2008a, A&A, 485, 917
 Ossenkopf, V., Krips, M., Stutzki, J., 2008b, A&A, 485, 719
 Padoan, P., Jones, J.T., Nordlund, A.A., 1997, ApJ, 474, 730
 Padoan, P., Juvela, M., Bally, J., Nordlund, A.A., 2000, ApJ 529, 259
 Piepenbrink, A., & Wendker, H.J., 1988, A&A, 191, 313
 Reipurth, B., Schneider, N., 2008, Handbook of low mass star forming regions, ASP, p.39
 Robin, A. C., Reyl  , C., Derri  re, S., Picaud, S., A&A, 2003, 409, 523
 Scalo, J.M., 1987, Proceedings of the Symposium, Grand Teton National Park. Dordrecht, D. Reidel Publishing Co., p.349.
 Schneider, N., & Brooks, K.J., 2004, PASA, 21, 290
 Schneider, N., Bontemps, S., Simon, R., Jakob, H., Motte, F., Miller, M., Kramer, C., Stutzki, J., 2006, A&A, 458, 855
 Schneider, N., Simon, R., Bontemps, S., Comer  n, F., Motte, F., 2007, A&A, 474, 873
 Simon, R., Jackson, J. M., Clemens, D. M., Bania, T. M., & Heyer, M.H. 2001, ApJ, 551, 747
 Stutzki, J., 2001, Astron. and Astrophys. Space Science Supp., 277, 39-49
 Stutzki, J., Bensch, F., Heithausen, A., Ossenkopf, V., Zielinsky, M., 1998, A&A, 336, 697
 Sun, K., Kramer, C., Ossenkopf, V., Bensch, F., Stutzki, J., A&A, 2006, 451, 539
 Tachihara, K., Neuh  user, R., Toyoda, S., 2001, Astr. Gesellschaft Abstract Series, Vol 18, p. 72
 Uyaniker, B., F  rst, E., Reich, W., Aschenbach, B., Wielebinski, R., 2001, A&A, 371, 675
 Vazquez-Semadeni, E., Ballesteros-Paredes, J., Rodriguez, L.F., 1997, ApJ 474, 292
 Vazquez-Semadeni, Gomez, G.C., Jappsen, A.K., et al., 2007, ApJ, 657, 870
 Vazquez-Semadeni, E., Gonzales, R.F., Ballesteros-Paredes, J., et al., 2008, MNRAS, 390, 769
 Williams J., Blitz L., Stark T., 1995, ApJ 451, 252